Utilizing the Neglected Back Lobe for Mobile Charging

Meixuan Ren*†, Dié Wu*†, Jing Xue*†, Wenzheng Xu‡, Jian Peng‡, Tang Liu*†
*College of Computer Science, Sichuan Normal University, Chengdu, Sichuan 610101, China
†Visual computing and virtual reality Key Lab, Sichuan Normal University, Chengdu, Sichuan 610068, China
‡College of Computer Science, Sichuan University, Chengdu, Sichuan 610065, China
Email: {meixuanren, xuejing}@stu.sicnu.edu.cn, {wd, liutang}@sicnu.edu.cn, {wenzheng.xu, jianpeng}@scu.edu.cn

IEEE INFOCOM 2023 - IEEE Conference on Computer Communications | 979-8-3503-3414-2/23/$31.00 ©2023 IEEE | DOI: 10.1109/INFOCOM53939.2023.10228855

***Abstract*—Benefitting from the breakthrough of wireless power transfer technology, the lifetime of Wireless Sensor Networks (WSNs) can be significantly prolonged by scheduling a mobile charger (MC) to charge sensors. Compared with omnidirectional charging, the MC equipped with directional antenna can concentrate energy in the intended direction, making charging more efficient. However, all prior arts ignore the considerable energy leakage behind the directional antenna (*i.e.,* back lobe), resulting in energy wasted in vain. To address this issue, we study a fundamental problem of how to utilize the neglected back lobe and schedule the directional MC efficiently. Towards this end, we first build and verify a directional charging model considering both main and back lobes. Then, we focus on jointly optimizing the number of dead sensors and energy usage effectiveness. We achieve these by introducing a scheduling scheme that utilizes both main and back lobes to charge multiple sensors simultaneously. Finally, extensive simulations and field experiments demonstrate that our scheme reduces the number of dead sensors by 49.5% and increases the energy usage effectiveness by 10.2% on average as compared with existing algorithms.**

***Index Terms*—Wireless power transfer, directional charging, back lobe, wireless rechargeable sensor networks**

I. Introduction

Energy limitation is widely recognized as a key hurdle that stunts the adoption of Wireless Sensor Networks (WSNs) [1], [2]. Recently, the breakthrough of wireless power transfer [3] technology gave birth to the concept of Wireless Rechargeable Sensor Networks (WRSNs) [4]–[6] and made it received widespread attention. In WRSNs, a mobile charger (MC) is usually employed to visit and recharge energy-critical sensors, such that the operational lifetimes of sensors can be significantly prolonged. Although WRSNs have many potentials in various application scenarios (*e.g.,* environmental monitoring [7], healthcare [8], and military [9]), there still exists a gap between energy supply and practical demand.

A key reason for this gap is that the energy radiated by MC is not fully utilized. Traditional wireless charging arts [10]–[17] usually employ omnidirectional antennas, which broadcast electromagnetic waves equally in all directions regardless of the location of the sensors, in this case, merely a small part of the energy could be transferred to the sensors. Instead, directional antennas concentrate the energy in the intended narrow direction via energy beamforming [18]–[26], and thus enhance the energy transferred to the sensors. Nevertheless, the energy radiated by MC is still underutilized, as an unignorable part of the energy is "leaking" in unintended directions for almost all directional antennas [27].

Corresponding author: **Tang Liu***† (Email: liutang@sicnu.edu.cn)

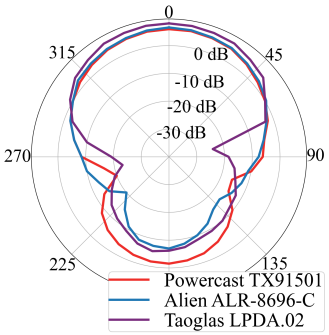

Fig. 1. Radiation patterns of three typical directional antennas produced by Powercast, Alien, and Taoglas.

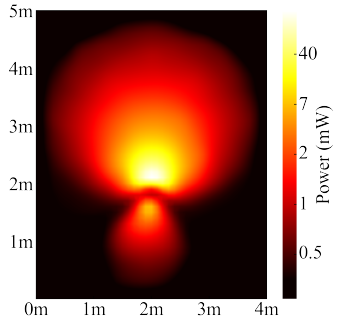

Fig. 2. A charging energy heatmap of TX91501 wireless charger produced by Powercast.

Fig. 1 depicts the radiation patterns of three typical commercial off-the-shelf directional antennas [28]–[30]. It shows that in front of each directional antenna, there is an energy beam with maximum energy intensity, *aka* the *main lobe* [27]. Besides, in other directions of each antenna, there are some smaller energy beams, also called the *side lobes*, among which the extremely important one directly behind the main lobe is the *back lobe* [27]. To further demonstrate the energy radiation pattern of directional antenna in different directions, we take Powercast TX91501 [28] as an example and plot its energy distribution in Fig. 2. It can be observed that the farthest charging distance of the back lobe is up to 50% of that of the main lobe. Moreover, the energy intensity of the back lobe is about 20% of that of the main lobe at the same transmission distance. Even though much effort has been devoted to concentrate all the radiated energy on the main lobe [31]–[33], energy leakage is inevitable. As a result, a considerable amount of energy leaking behind the directional antenna is wasted in vain.

Although there are some arts focusing on the directional charging scheduling [19]–[21], none of them pay attention to the back lobe. All these studies design charging scheduling schemes according to the charging range and energy intensity of the main lobe. Therefore, these schemes do not effectively utilize the leaked energy behind the MC. Assuming that both the main and back lobes are utilized, in this case, a larger

charging range of the MC means that more sensors have a greater chance to be charged simultaneously, thereby reducing the number of dead sensors. Meanwhile, more radiated energy from the MC can be received by sensors, thus improving the energy usage effectiveness (*EUE*). In summary, it is necessary to model the charging range and energy intensity of both the main and back lobes, and accordingly design a charging scheduling algorithm.

In this paper, we focus on making full use of the energy of the main and back lobes to improve charging performance. In particular, we study the problem of directional charging scheduling with main and BACK lobes (BACK), *i.e.,* how to use a directional MC to travel and stop at several candidate locations with proper orientations to charge sensors so that the number of dead sensors is minimized and *EUE* is maximized. Generally, we are faced with two major challenges.

The first challenge is how to build a charging model with both main and back lobes that accurately describes the characteristics of the directional MCs. Unlike the main lobe, the manufacturers do not provide the parameters of the back lobe because it is regarded as useless, or even troublesome, which raises challenges in modeling energy transfer. In addition, for different antennas, the radiation pattern of the back lobe varies, the established model should be general and accurate enough for most commercial off-the-shelf directional antennas.

The second challenge is how to design an effective scheduling algorithm for BACK. With respect to energy constraints, scheduling the charging path of MC is similar to solving an NP-hard traveling salesman problem (TSP). Moreover, the MC can freely adjust its orientation in $[0, 2\pi)$, which means the number of candidate orientations for MC to choose is infinite. Note that, since the energy intensity and charging range of the back lobe are different from those of the main lobe, it is more difficult to determine not only when and where to sojourn for an MC, but its orientation.

To summarize, our contributions in this paper are as follows:

- To the best of our knowledge, this is the first work to utilize both the main and back lobes to wireless charge sensors. We build a charging model with main and back lobes, which can accurately model the energy radiated by MC. In addition, this model can be reduced to a keyhole model suitable for most directional antennas.
- To solve the BACK problem, we propose a charging scheme. We show that our scheme approximates the optimal number of dead sensors with a ratio of $max\{\frac{\beta^2}{(D_m+\beta)^2}, \frac{1}{\sqrt{2}(\sqrt{N}+1)}\}$ and the optimal *EUE* with a ratio of $\sqrt{N_l}$, where D_m and β are constants determined by the environment and the hardware parameters of chargers, N and N_l are the number of sensors and sojourn locations in the scheme, respectively.
- To evaluate our scheme, we conduct simulations and field experiments to demonstrate that on average, our scheme reduces the number of dead sensors by 49.5% and increases *EUE* by 10.2% compared to existing algorithms.

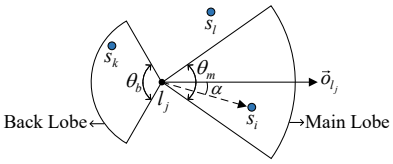

Fig. 3. Directional charging model with main and back lobes.

II. Modeling

A. Network Model

Consider a 2D plane network (with side length L_n) with a base station (BS), N stationary sensors $S = \{s_1, s_2, ..., s_N\}$, M candidate sojourn locations $L = \{l_1, l_2, ..., l_M\}$, and a directional MC with battery capacity B. Each sensor s_i is powered by a rechargeable battery with capacity b. Let re_i and ec_i denote the residual energy and energy consumption rate of s_i, respectively, so its residual lifetime is re_i/ec_i.

As the network operates, sensors consume their battery energy. When the residual lifetime of a sensor is lower than a given threshold θ_l, it will send a charging request $\boldsymbol{REQ}_i = (t, s_i, re_i, ec_i)$ to BS, where $\boldsymbol{REQ}_i$ contains the time point t, the sensor ID s_i, its residual energy re_i, and its energy consumption rate ec_i.

According to the received charging requests, a *charging path* is constructed by BS. In one *charging cycle*, MC departs from BS with full energy, then it moves along the charging path to visit some selected sojourn locations in some order and charges sensors wirelessly. We define the strategy of the MC as a tuple $\langle l_j, \overrightarrow{o_{l_j}} \rangle$ that denotes the sojourn location l_j and orientation $\overrightarrow{o_{l_j}}$ of the MC. Only the sensors located in the main or back lobe can receive non-negligible energy. Before MC exhausts its energy, it returns to BS and gets recharged for the next charging cycle.

B. Charging Model

We build our directional charging model based on empirical studies and field experiments. The testbed consists of a commodity off-the-shelf wireless charger TX91501 produced by Powercast [28], and a rechargeable sensor equipped with an omnidirectional antenna. We place the sensor around the charger from near to far and record the received energy. The experimental results are depicted in Fig. 2, which reveals two insights: (1) the farthest charging distance behind the charger is half of that in front of the charger (*i.e.,* $1.3m$ and $2.6m$); (2) the beamwidth of the back lobe is different from that of the main lobe (*i.e.,* $2\pi/3$ and $\pi/3$).

Therefore, we propose the directional charging model with main and back lobes as shown in Fig. 3, which generalizes the traditional directional charging model [21], [22]. For simplicity, we build a double-sector model to approximate the radiation pattern of realistic antennas. Hence, the charging range of the main and back lobes are each modeled as a sector. We apply the farthest charging distance as the radius, and the beamwidth as the angle of the sectors. Consequently, it can be seen in Fig. 3, when the orientation of charger is $\overrightarrow{o_{l_j}}$, s_i and s_k with in charging range can be replenished, while the energy received by s_l is negligible.

In practice, since the back lobe is the energy beam of the antenna, the Friis's free space equation is also feasible in it. Therefore, by incorporating the widely accepted empirical charging model proposed in [10], [11], [22], the charging power transmitted from the charger to a sensor s_i can be given by:

$$PR(d) = \frac{G_t G_r \eta}{L_p}(\frac{\lambda}{4\pi(d+\beta)})^2 PT, \tag{1}$$

where d is the distance between the charger and s_i, η is the rectifier efficiency, L_p is the polarization loss, λ is the average wavelength, β is a parameter to adjust the Friis's free space equation for the short distance transmission, and PT refers to the transmission power of the charger. Moreover, G_t and G_r represent the transmit gain and the receive gain, respectively.

Since sensors are equipped with an omnidirectional antenna, the receive gain G_r is an angle-independent constant. In contrast, the transmit gain G_t is a function of angle, which is defined as the ratio of the radiation intensity in a given direction to the radiation intensity produced by the omnidirectional antenna at the same power, so G_t can be expressed in a spherical coordinate system as:

$$G_t(\theta, \phi) = \eta \frac{U(\theta, \phi)}{U_o}, \tag{2}$$

where η is set to be 1 since antennas are often assumed to be lossless [34]. θ is the elevation angle from the z-axis within $[0, \pi]$, ϕ is the azimuth angle from the x-axis within $[0, 2\pi]$. $U(\theta, \phi)$ and U_o are respectively the radiation intensity of directional and omnidirectional antennas at the same power, that is, the power per unit solid angle.

For the omnidirectional antenna, it radiates power equally in all directions, so we can obtain the total transmission power of the antenna, PT, by integrating U_o over the steradian Ω:

$$PT = \oiint_{\Omega} U_o \mathrm{d}\Omega = U_o \oiint_{\Omega} \mathrm{d}\Omega = 4\pi U_o. \tag{3}$$

For the directional antenna, we place it in the center of the spherical coordinate system. Let θ_0 denote the elevation angle of the direction for power concentration, in other words, the main lobe will be targeted in the direction of the elevation angle θ_0. Since PT is the sum of the power of all unit solid angles in the spherical coordinate system, it can also be expressed as the integral over the entire area of the $U(\theta, \phi)$:

$$PT = \oiint_{\Omega} U(\theta, \phi) \mathrm{d}\Omega = \int_0^{2\pi}\int_0^{\pi} U(\theta, \phi) \sin\theta \mathrm{d}\theta \mathrm{d}\phi. \tag{4}$$

By combining Eq. (2) and Eq. (4), the expression of PT with respect to the transmit gain G_t is obtained:

$$PT = \int_0^{2\pi}\int_0^{\pi} G_t(\theta, \phi) U_o \sin\theta \mathrm{d}\theta \mathrm{d}\phi. \tag{5}$$

Considering that the radiation intensity of the back lobe is different from that of the main lobe, we use a piecewise constant function to describe the transmit gain function $G_t(\alpha)$:

$$G_t(\alpha) = \begin{cases} G_m, & -\frac{\theta_m}{2} \le \alpha \le \frac{\theta_m}{2}, \\ G_b, & \pi - \frac{\theta_b}{2} \le \alpha \le \pi + \frac{\theta_b}{2}, \\ 0, & \text{otherwise}, \end{cases} \tag{6}$$

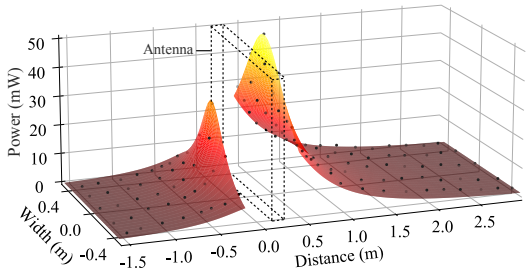

Fig. 4. Comparing experimental data (black dots) and fitted data (mesh). Fitted results are based on $\mu = 0.31$, $\beta = 0.053$, $G_m = 8$, and $G_b = 1.856$.

where α is the relative angle between the charger and the sensor. When α is within beamwidth θ_m of the main lobe, the value of $G_t(\alpha)$ is equal to the main lobe gain G_m. Similarly, when α is within beamwidth θ_b of the back lobe, its value is equal to the back lobe gain G_b. As shown in Fig. 2, the transmission power of the charger consists of two parts: the main lobe part denoted by PT_m and the back lobe part denoted by PT_b. In the same way, they can be expressed as:

$$PT_m = \int_0^{2\pi}\int_0^{\frac{\theta_m}{2}} G_m U_o \sin\theta \mathrm{d}\theta \mathrm{d}\phi. \tag{7}$$

$$PT_b = \int_0^{2\pi}\int_{\pi-\frac{\theta_b}{2}}^{\pi} G_b U_o \sin\theta \mathrm{d}\theta \mathrm{d}\phi. \tag{8}$$

Although the type of radiation is different, the transmission power is the same, so we have:

$$4\pi U_o = \int_0^{2\pi}\int_0^{\frac{\theta_m}{2}} G_m U_o \sin\theta \mathrm{d}\theta \mathrm{d}\phi + \int_0^{2\pi}\int_{\pi-\frac{\theta_b}{2}}^{\pi} G_b U_o \sin\theta \mathrm{d}\theta \mathrm{d}\phi. \tag{9}$$

The G_b can be obtained directly from the above equation:

$$G_b = \frac{2 - G_m(1 - cos(\frac{\theta_m}{2}))}{1 + cos\frac{\theta_b}{2}}, \tag{10}$$

in particular, when $\theta_b = 2\pi - \theta_m$, the double-sector model becomes the keyhole model that approximates all energy beams except the main lobe as a sector, which is suitable for most commercial directional antennas [35], [36]. Actually, for off-the-shelf chargers, manufacturers only provide the value of the main lobe gain G_m, not the back lobe gain G_b, because it is regarded as useless. But we can calculate it by Eq. (10).

In conclusion, the charging power transmitted from the MC to a sensor s_i is updated as:

$$PR(d, \alpha) = \begin{cases} \frac{G_m \mu}{(d+\beta)^2}, 0 \le d \le D_m, -\frac{\theta_m}{2} \le \alpha \le \frac{\theta_m}{2}, \\ \frac{G_b \mu}{(d+\beta)^2}, 0 \le d \le D_b, \pi - \frac{\theta_b}{2} \le \alpha \le \pi + \frac{\theta_b}{2}, \\ 0 \qquad \text{otherwise}, \end{cases} \tag{11}$$

where d and α refer to the distance and relative angle between MC and s_i, respectively. To simplify the expression, we set $\mu = \frac{G_r \eta}{L_p}(\frac{\lambda}{4\pi})^2 PT$ to represent some parameters. μ, G_m, and β are constants determined by the environment and the hardware parameters of chargers, G_b can be calculated by Eq. (10).

To further validate our charging model, we adopt Eq. (11) to fit the field experimental data in Fig. 2. The fitting results are shown in Fig. 4. It can be seen that the field experimental data

are consistent with the fitting data of Eq. (11), which proves that the directional charging model with main and back lobes is feasible in our experimental environment.

C. Problem Formulation

In a WSN, the deployed sensors perform various important tasks, such as sensing, collecting, and processing information. Once the sensor energy is exhausted, the WSN can no longer cover all monitoring areas and maintain its connectivity, potentially leading to the breakdown of the network. Therefore, our primary objective is to minimize the number of dead sensors.

Meanwhile, the battery capacity of the employed MC in a WRSN is limited. To make the energy-limited MC serve more sensors, the battery capacity of MC should be fully utilized to ensure that as much energy as possible replenishes to sensors. So our secondary objective is to maximize energy usage effectiveness (*EUE*), which is defined as follows:

$$EUE = \frac{E^{pl}}{E^{pl} + E^{tr} + E^{lo}}, \tag{12}$$

where E^{pl} is the energy eventually obtained by sensors, E^{tr} is the energy consumed to travel among sojourn locations, and E^{lo} is the energy loss during charging.

In this work, we study the problem of directional charging scheduling with main and BACK lobes (BACK): how to carefully choose appropriate sojourn locations and orientations for directional MC with limited energy to make full use of the energy radiated by its main and back lobes, so as to jointly optimize the number of dead sensors and *EUE*.

However, there exists a tradeoff between these two objectives [11] for the following reasons: to reduce the number of dead sensors, the MC needs to simultaneously charge sensors as much as possible to meet their charging requests. But this may lead to long-distance charging, resulting in a lower *EUE*. On the other hand, improving the *EUE* requires the MC to approach each sensor in close proximity to charge them at a very short distance. Obviously, that in turn makes it difficult to ensure that there are sufficient sensors in the MC's charging range, increasing the number of dead sensors. Therefore, we first minimize the number of dead sensors, based on which we further maximize the *EUE*.

Problem 1. *The primary objective is to find a directional charging scheme that utilizes both the main lobe and back lobe to minimize the number of dead sensors in one charging cycle, under the constraint of limited battery capacity and charging range of the MC, i.e.,*

$$\text{minimize} \quad N_{ds}, \tag{13}$$

subject to

$$E^{pl} + E^{tr} + E^{lo} \le B, \tag{14}$$

$$\begin{aligned} &0 \le d \le D_m, -\frac{\theta_m}{2} \le \alpha \le \frac{\theta_m}{2}, \\ \text{or} \quad &0 \le d \le D_b, \pi - \frac{\theta_b}{2} \le \alpha \le \pi + \frac{\theta_b}{2}. \end{aligned} \tag{15}$$

Problem 2. *The secondary objective is to find a directional charging scheme that maximizes energy usage effectiveness under the constraint of the minimum number of dead sensors, i.e.,*

$$\text{maximize} \quad EUE, \tag{16}$$

subject to

$$N_{ds} = N_{ds}^{*}, \tag{17}$$

where N_{ds}^{*} is the minimum number of dead sensors.

III. Solution

In this section, to tackle the BACK problem, we propose a scheme composed of four algorithms, among which Alg. 1, 2, and 3 together achieve the objective of minimizing the number of dead sensors, on the basis of the minimized number of dead sensors, Alg. 4 further maximizes the *EUE*.

A. Initial Path Planning Algorithm

First, we propose an initial path planning algorithm for providing a feasible charging scheduling. In order to achieve our primary objective of minimizing the number of dead sensors, we should schedule the MC to preferentially charge the sensor with urgent charging requests. Accordingly, the basic idea of Alg. 1 is to greedily select the energy-critical sensor with the shortest residual lifetime for charging service in each iteration. When a sensor cannot be charged before its deadline, we will try to charge it by changing the charging order. If it fails, we will adjust the MC's orientation or replace the sojourn location in the charging path to incidentally replenish energy to the dropped sensor while serving other sensors. The detailed process is demonstrated in Alg. 1.

Algorithm 1: Initial Path Planning algorithm

Input: A to-be-charged queue Q_t and a set of pre-determined sojourn locations L
Output: An initial charging path P' and the set of dead sensors $N_d(s)$

Sort all charging requests in Q_t in increasing order of their deadlines;
for *each sensor* s_i *in* Q_t **do**
  Select the nearest sojourn location l_i to sensor s_i;
  Orientation $\overrightarrow{o_{l_i}}$ is facing s_i (*i.e.,* $\overrightarrow{o_{l_i}} = \overrightarrow{l_i s_i}$);
  if $t_{l_i}^{arr} \le TD(s_i)$ **then**
    Add $\langle l_i, \overrightarrow{o_{l_i}} \rangle$ to the tail of P', continue;
  Try to insert $\langle l_i, \overrightarrow{o_{l_i}} \rangle$ into P' as the fth strategy $(1 \le f \le |P'|)$;
  if *the insert fails* **then**
    Call Algorithm 2 to rescue s_i;
    if $t_{l_i}^{arr} > TD(s_i)$ **then**
      Call Algorithm 3 to optimize P';
      if $t_{l_i}^{arr} > TD(s_i)$ **then**
        $N_d(s) \leftarrow N_d(s) \cup \{s_i\}$;
Return the initial charging path P';

Alg. 1 proceeds as follows. At first, we sort the N_r charging requests in the to-be-charged queue Q_t in increasing order of their deadlines. Shorter deadline indicates higher charging priority. That is, suppose the sorted sequence is $REQ_1, REQ_2, ..., REQ_{N_r}$, it means $TD_1 \leq TD_2 \leq ... \leq TD_{N_r}$. Denote s_i by the sensor which sends charging request REQ_i. When trying to add s_i to the charging path, we preferentially select the nearest candidate sojourn location to s_i, and by default, the MC is facing s_i. Here, we also let l_i and $\overrightarrow{o_{l_i}}$ denote by the corresponding sojourn location and the MC's orientation respectively when the MC serves s_i, which together constitute the strategy $\langle l_i, \overrightarrow{o_{l_i}} \rangle$. We then gradually construct an initial charging path $P' = (\langle l_1, \overrightarrow{o_{l_1}} \rangle, \langle l_2, \overrightarrow{o_{l_2}} \rangle, ..., \langle l_{N_r}, \overrightarrow{o_{l_{N_r}}} \rangle)$ by adding $\langle l_i, \overrightarrow{o_{l_i}} \rangle$ to a partial charging path. Meanwhile, since all sensors within the charging range will be charged at the same time, we update the deadlines of all sensors covered by l_i, including s_i, after $\langle l_i, \overrightarrow{o_{l_i}} \rangle$ has been added into the charging path. Then, the charging requests in Q_t will be updated too.

For any sensor s_i, if the deadline TD_i is less than the time $t_{l_i}^{arr}$ when the MC arrives at its sojourn location l_i, it means that s_i cannot be charged in time. We call such sensor s_i as "dropped sensor" and it needs re-arranging a former position. Hence, we scan each former strategy to find a proper place to insert $\langle l_i, \overrightarrow{o_{l_i}} \rangle$. For a former strategy $\langle l_f, \overrightarrow{o_{l_f}} \rangle (1 \leq f < i)$, if inserting $\langle l_i, \overrightarrow{o_{l_i}} \rangle$ to the front of it will not cause other sensors dead, we insert $\langle l_i, \overrightarrow{o_{l_i}} \rangle$ in the front of $\langle l_f, \overrightarrow{o_{l_f}} \rangle$. Otherwise, we cannot rescue the dropped sensor s_i by only changing the charging order. In this case, Alg. 2 and 3 will be called in turn to optimize the current P'. Once the dropped sensor s_i cannot be rescued by calling both Alg. 2 and 3, s_i will be eventually added into the set of dead sensors $N_d(s)$. Then, Alg. 1 continues to construct the charging path until all to-be-charged sensors are tried to join the path P'.

B. Dropped Sensor Rescue Algorithm

As demonstrated in line 9 of Alg. 1, we use Alg. 2 to rescue the dropped sensor s_i for further minimizing the number of dead sensors. The basic idea is to use the energy radiated from the back lobe of the MC to incidentally charge s_i while the MC serves other sensors, so as to prolong the residual lifetime of s_i. Since the MC can arbitrarily adjust its orientation at each sojourn location, we first try to change the orientation in the initial charging path so that s_i can be incidentally charged. Fig. 5 shows an example of rescuing the dropped sensor by rotating the MC. It can be seen that when the MC charges s_j with the default orientation, there is a dropped sensor s_i located outside the charging area of the MC. If we rotate the MC clockwise from $\overrightarrow{o_{l_j}}$ to $\overrightarrow{o'_{l_j}}$, s_i will be replenished energy from the back lobe of the MC while the MC charges s_j.

If s_i cannot be rescued by adjusting the orientation, another feasible method is to select a sensor s_j in the initial path and try to replace its corresponding sojourn location with one that can simultaneously cover both s_i and s_j. As shown in Fig. 6, when the MC serves s_j, its default sojourn location is l_j, which is the nearest to s_j. Because $\angle s_j, l_j, s_i \in (\theta_m, \pi - \frac{\theta_m + \theta_b}{2})$, s_i and s_j cannot be simultaneously located within the charging range by rotating the MC. If we replace l_j with another candidate sojourn location l'_j, and determine an appropriate orientation, s_i and s_j will be charged simultaneously. Based on the above observations, we design Alg. 2.

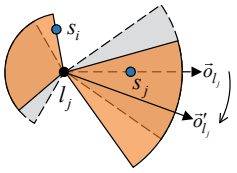

Fig. 5. An example of adjusting the MC's orientation.

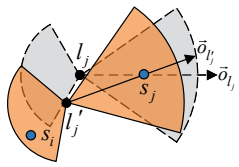

Fig. 6. An example of replacing the sojourn location.

Alg. 2 proceeds as follows. First, we call all sensors in P' whose distance from the dropped sensor s_i is not greater than $D_m + D_b$ as neighbors of s_i. We denote by $\mathcal{S}^N(s_i)$ the set of neighbors of s_i and sort these neighbors in increasing order of the distance from s_i (*i.e.*, $d_{s_1^N(s_i), s_i} < d_{s_2^N(s_i), s_i} < ...$). Then, we scan each neighbor $s_j^N(s_i)$ in $\mathcal{S}^N(s_i)$ to determine whether the distance between its corresponding sojourn location $l_j^N(s_i)$ and s_i is not greater than D_m. If so, we will try to adjust its corresponding orientation to rescue s_i. The adjustment can be divided into two cases: (*i*) when $\angle s_j^N(s_i), l_j^N(s_i), s_i \leq \theta_m$, the MC is rotated in the direction close to s_i until reaching s_i on the boundary of the main lobe; (*ii*) when $\angle s_j^N(s_i), l_j^N(s_i), s_i \geq \pi - \frac{\theta_m + \theta_b}{2}$, the MC is rotated in the opposite direction from s_i until reaching s_i on the boundary of the back lobe. After adjusting the orientation, when two premise conditions: a) s_i can survive until it is added to P'; b) it will not cause other sensors dead, are both satisfied, we will update $\langle l_j^N(s_i), \overrightarrow{o_{l_j^N(s_i)}} \rangle$ in P' and add $\langle l_i, \overrightarrow{o_{l_i}} \rangle$ to P'.

When s_i cannot be rescued by adjusting the orientation, we will try to rescue it by replacing an existing sojourn location in P' with a new candidate sojourn location. We scan each neighbor $s_j^N(s_i)$ in $\mathcal{S}^N(s_i)$ to determine whether there is a nearby candidate sojourn location l_j^* that can cover both

Algorithm 2: Dropped Sensor Rescue algorithm

Input: A charging path P' and a strategy $\langle l_i, \overrightarrow{o_{l_i}} \rangle$ corresponding to the dropped sensor s_i
Output: An optimized path P'

1 Sort all neighbors in $\mathcal{S}^N(s_i)$ in increasing order of the distance from s_i;
2 **for** *each neighbor* $s_j^N(s_i)$ *in* $\mathcal{S}^N(s_i)$ **do**
3 **if** $d_{l_j^N(s_i), s_i} \leq D_m$ **then**
4 Aadjust the orientation $\overrightarrow{o_{l_j^N(s_i)}}$ until reaching s_i on the boundary of the charging area;
5 Update the strategy $\langle l_j^N(s_i), \overrightarrow{o_{l_j^N(s_i)}} \rangle$ in P';
6 **if** $t_{l_i}^{arr} \leq TD(s_i)$ **then**
7 Add $\langle l_i, \overrightarrow{o_{l_i}} \rangle$ to the tail of P', return P';
8 **for** *each neighbor* $s_j^N(s_i)$ *in* $\mathcal{S}^N(s_i)$ **do**
9 **for** *each sojourn location* l_j^* *in* L **do**
10 **if** l_j^* *can cover* s_i *and* s_j **then**
11 Add $\langle l_i, \overrightarrow{o_{l_i}} \rangle$ to the tail of P', return P';
12 Return the optimized charging path P';

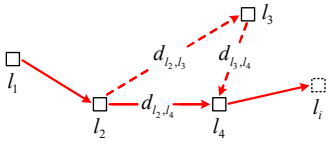

Fig. 7. An example of optimizing charging path.

(a) An initial charging path (b) An exchanging-based optimized path

Fig. 8. An example of exchanging two sojourn locations to improve *EUE*.

$s_j^N(s_i)$ and s_i, and judge whether two premise conditions mentioned above are both satisfied when MC is scheduled to l_j^*. If so, we will replace $\langle l_j^N(s_i), \overrightarrow{o_{l_j^N(s_i)}}\rangle$ with $\langle l_j^*, \overrightarrow{o_{l_j^*}}\rangle$, update the deadline of all sensors in P', and add $\langle l_i, \overrightarrow{o_{l_i}}\rangle$ to the tail of P'. If there is no candidate sojourn location near all neighbor sensors in $\mathcal{S}^N(s_i)$ that can rescue s_i, Alg. 3 will be called to optimize P'.

C. Charging Path Optimization Algorithm

As demonstrated in line 11 of Alg. 1, when the dropped sensor s_i cannot be rescued by calling Alg. 2, we use Alg. 3 to optimize the initial charging path. Our optimization objective is to preserve more time for subsequent scheduling, so that the MC can charge the sensors in the to-be-charged queue Q_t as soon as possible. Since the traveling cost of MC moving to each sojourn location is not equal, an effective way to shorten the length of the charging path is to replace the sojourn location l_{tr}^{max}, which has the highest traveling cost in P', with the sojourn location l_i corresponding to the dropped sensor s_i. For the replacement, the following two conditions should be satisfied: (*i*) the number of dead sensors brought by removing l_{tr}^{max} will not be greater than one; (*ii*) after deleting l_{tr}^{max}, s_i can be added to the charging path before its deadline, and the new path has less total traveling cost T_{total}.

We use an example to illustrate how to optimize the charging path by replacing sojourn locations. As shown in Fig. 7, $P = (\langle l_1, \overrightarrow{o_{l_1}}\rangle, \langle l_2, \overrightarrow{o_{l_2}}\rangle, \langle l_3, \overrightarrow{o_{l_3}}\rangle, \langle l_4, \overrightarrow{o_{l_4}}\rangle)$ is the initial charging path. It can be seen that l_3 is far away from its adjacent sojourn locations l_2 and l_4, so l_3 has the highest traveling cost. Obviously, removing l_3 can not only significantly shorten the length of the charging path, but also make it probable for MC to have a great chance to charge the dropped sensor s_i before its deadline. Here, we use Eq. (18) to find the sojourn location l_{tr}^{max} with the highest traveling cost in P':

$$l_{tr}^{max} = \underset{l_j \in P'}{arg\ max}\ (d_{l_{j-1},l_j} + d_{l_j,l_{j+1}} - d_{l_{j-1},l_{j+1}}). \quad (18)$$

Alg. 3 proceeds as follows. We scan the constructed charging path P' to find l_{tr}^{max}. Then, we remove l_{tr}^{max} and connect its two adjacent sojourn locations.

Subsequently, we scan the connected path for an appropriate position to insert the $\langle l_i, \overrightarrow{o_{l_i}}\rangle$ corresponding to s_i. If the new path satisfies the two replacement conditions mentioned above, we will add the sensor corresponding to l_{tr}^{max} to $N_d(s)$. Otherwise, l_{tr}^{max} will be added back to P' and s_i will be added to $N_d(s)$.

D. EUE Optimization Algorithm

After the initial charging path P' is contracted, we concentrate on the secondary objective: how to maximize the energy usage effectiveness (*EUE*). Recall that the total energy consumption of the MC consists of three parts: the energy obtained by sensors E^{pl}, the traveling energy consumption E^{tr}, and the energy loss during charging E^{lo}. According to Eq. (11) and (12), to achieve the maximal *EUE*, two following factors should be considered based on its definition: (*i*) shorter traveling length results in greater *EUE*; (*ii*) shorter charging distance also leads to greater *EUE*.

Algorithm 3: Charging Path Optimization algorithm

Input: A charging path P' and a strategy $\langle l_i, \overrightarrow{o_{l_i}}\rangle$ corresponding to the dropped sensor s_i
Output: An optimized path P'

$P_{temp} \leftarrow P'$;
for *any three adjacent sojourn locations* l_a, l_b, l_c **do**
  $f(l_b) = d_{l_a,l_b} + d_{l_b,l_c} - d_{l_a,l_c}$;
$l_b^* \leftarrow arg\ max\ f(l_b)$;
Remove strategy $\langle l_b^*, \overrightarrow{o_{l_b^*}}\rangle$ from P_{temp};
Connect l_a^* and l_c^* in P_{temp};
for $f \leftarrow |P_{temp}|$ *to 1* **do**
  Select $\langle l_i, \overrightarrow{o_{l_i}}\rangle$ as the fth strategy to join P_{temp};
  if $N_{ds}(P_{temp}) == N_{ds}(P')$ *AND* $T_{total}(P_{temp}) < T_{total}(P')$ **then**
    $P' \leftarrow P_{temp}, N_d(s) \leftarrow N_d(s) \cup \{s_i\}$, break;
  else
    Remove the fth strategy from P_{temp};
Return the optimized charging path P';

Algorithm 4: *EUE* Optimization algorithm

Input: An initial charging path P' and the $EUE_{P'}$ obtained by the MC in P'
Output: A final charging path P and the EUE_P obtained by the MC in P

$P_{temp} \leftarrow P'$;
for $count \leftarrow 0$ *to* $\mathcal{M}$ **do**
  Randomly select two sojourn locations l_i and $l_j (i < j)$ from P_{temp};
  Take the sub-path from l_1 to l_{i-1} and add it in order to P_{temp};
  Take the sub-path from l_i to l_j and add them in reverse order to P_{temp};
  Add the sub-path from l_{j+1} to l_{N_l} in order to P_{temp};
  if $N_{ds}(P_{temp}) == N_{ds}(P')$ *AND* $EUE(P_{temp}) > EUE(P')$ **then**
    $P' \leftarrow P_{temp}, count \leftarrow 0$;
  else
    $P_{temp} \leftarrow P', count \leftarrow count + 1$;
Return the final charging path P;

We use an example to demonstrate how can we achieve the maximal *EUE* by jointly considering these two factors. Fig. 8(a) gives the initial charging path and its charging order is BS$\rightarrow l_1 \rightarrow l_2 \rightarrow l_3 \rightarrow l_4 \rightarrow l_5 \rightarrow$BS. It can be seen that s is located at the overlapping charging area of l_3 and l_4. Assume that the residual energy of s is relatively more, it can be fully charged no matter whether MC is staying at l_3 or l_4.

Intuitively, if we exchange the charging order of l_3 and l_4, not only the charging path length can be reduced significantly, but s can be fully charged with a shorter charging distance when MC is staying at l_4. The scheduling result of the optimized charging path is shown in Fig. 8(b).

From this example, it can be seen that exchanging the charging order of the initial path can jointly address the two factors mentioned above. Inspired by this observation, we design Alg. 4, a charging order exchanging-based optimization algorithm, to maximize the *EUE*.

Alg. 4 proceeds as follows. Assume there are total N_l sojourn locations in P'. We randomly select two sojourn locations l_i and $l_j (i < j)$ from P'. Then we rearrange the sub-path from l_i to l_j in reverse order while the other sub-paths remain in the same order, together forming a temporary path P_{temp}. If compared with P', P_{temp} has the same number of dead sensors and a higher *EUE*, we will assign P_{temp} to P'. These process will be repeated until a continuous $\mathcal{M}$-times exchange of two randomly selected sojourn locations cannot lead to further improvement of *EUE*.

IV. THEORETICAL ANALYSIS

Recall that the essential purpose of Alg. 1 is to construct a charging path for the MC that minimizes the number of dead sensors. Hence, we sort the charging requests received by BS in increasing order of their urgency. In each iteration, we greedily selected the sensor with the most urgent charging request and added it to the charging path. To bound the performance, we present the approximation ratio analysis.

Theorem 1. *The Alg. 1 delivers an approximate solution to the dead sensors minimization problem with the approximation ratio of* $max\{\frac{\beta^2}{(D_m+\beta)^2}, \frac{1}{\sqrt{2}(\sqrt{N}+1)}\}$.

Proof: Consider a special case of Alg. 1 that sensors are evenly distributed in the network. First, we analyze the relationship between the energy consumed by the MC and its battery capacity. For the optimal solution, we have:

$$E_{opt}^{pl} + E_{opt}^{tr} + E_{opt}^{lo} \leq B. \tag{19}$$

Note that, when the MC stays at a sojourn location, its transmitted power *PT* is spent on two parts, one part is obtained by sensors and the other part is lost during the charging process. Suppose that the charging duration of MC at each sojourn location and traveling distance between sojourn locations are evenly distributed, the average charging duration is denoted as T_{opt}^{avg}, and the average traveling distance is denoted as d_{opt}^{avg}, we have the following equation:

$$(N - N_{ds}^*) \cdot (\boldsymbol{PT} \cdot T_{opt}^{avg} + d_{opt}^{avg} \cdot c) \leq B, \tag{20}$$

where N is the number of sensors in the network, N_{ds}^* is the number of dead sensors in the optimal solution, and c is the energy consumed by traveling one unit distance.

Similarly, for our approximated solution, we have:

$$(N - N'_{ds}) \cdot (\boldsymbol{PT} \cdot T_{appr}^{avg} + d_{appr}^{avg} \cdot c) \leq B, \tag{21}$$

where N'_{ds} is the number of dead sensors in the approximated solution, which is the output of Alg. 1.

Here, we consider the best case for the optimal solution: all sensors are charged close enough to the MC, and the MC visits each sojourn location with the shortest traveling distance, *i.e.,* the uniform interval of adjacent sojourn locations. So we replace T_{opt}^{avg} and d_{opt}^{avg} by $\frac{b\beta^2}{G_m\mu}$ and $\frac{L_n}{\lceil\sqrt{N}\rceil}$. For the approximated solution, we greedily select the sensor with the shortest residual lifetime to charge it in each iteration. Consider the worst case, *i.e.*, all sensors are located at the farthest part of the charging area of the MC and the MC visits each sojourn location with the maximum traveling distance. So we replace T_{appr}^{avg} and d_{appr}^{avg} by $\frac{b(D_m+\beta)^2}{G_m\mu}$ and $\sqrt{2}L_n$, we have:

$$(N - N_{ds}^*) \cdot (\boldsymbol{PT} \cdot \frac{b\beta^2}{G_m\mu} + \frac{L_n}{\lceil\sqrt{N}\rceil} \cdot c) \leq B, \tag{22}$$

$$(N - N'_{ds}) \cdot (\boldsymbol{PT} \cdot \frac{b(D_m+\beta)^2}{G_m\mu} + \sqrt{2}L_n \cdot c) \leq B. \tag{23}$$

By combining Eq. (22) and Eq. (23), we have:

$$\begin{aligned} \frac{N_{ds}^*}{N'_{ds}} \leq \frac{(N - N_{ds}^*)}{(N - N'_{ds})} &\leq \frac{\boldsymbol{PT} \cdot \frac{b\beta^2}{G_m\mu} + \frac{L}{\lceil\sqrt{N}\rceil}c}{\boldsymbol{PT} \cdot \frac{b(D_m+\beta)^2}{G_m\mu} + \sqrt{2}Lc} \\ &\leq max\{\frac{\beta^2}{(D_m+\beta)^2}, \frac{1}{\sqrt{2}(\sqrt{N}+1)}\}. \end{aligned} \tag{24}$$

Therefore, the number of dead sensors obtained by our solution is smaller than $max\{\frac{\beta^2}{(D_m+\beta)^2}, \frac{1}{\sqrt{2}(\sqrt{N}+1)}\}$ of the optimal solution, and Theorem 1 is proved. ■

In Alg. 1, when a sensor cannot be charged in time, Alg. 2 and 3 will be called in turn to rescue it, eventually constructing an initial charging path. Our secondary objective is to maximize the *EUE* under the constraint that the number of dead sensors is minimized, so we designed Alg. 4 to maximize the *EUE* of the initial charging path. We show the approximate ratio analysis of Alg. 4 and the corresponding proof.

Theorem 2. *The Alg. 4 delivers an approximate solution to the EUE maximization problem with the approximation ratio of roughly* $\sqrt{N_l}$.

Proof: To maximize the *EUE*, Alg. 4 will try to exchange the charging order of two selected sojourn locations. We notice the basic idea of this solution is similar to the 2-opt algorithm [37], which is perhaps the most widely used local search algorithm for the Traveling Salesman Problem. By deleting two edges of the path and reconnecting them in the other possible way, 2-opt can find the shortest path. Following a theoretical derivation similar to that shown in [38], we can prove that Alg. 4 achieves an expected approximation ratio of roughly $\sqrt{N_l}$, where N_l is the number of sojourn locations in the charging path. Here, we omit the proof but refer readers to [38] for details. ■

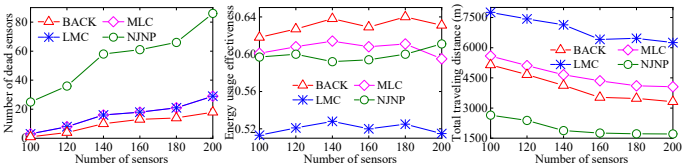

(a) N_{ds} (b) *EUE* (c) L^{tr}

Fig. 9. Performance comparisons by varying the number of sensors.

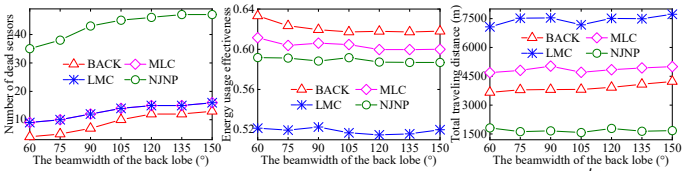

(a) N_{ds} (b) *EUE* (c) L^{tr}

Fig. 10. Performance comparisons by varying θ_b.

V. Simulations

A. Simulation Setup

We consider a WRSN consisting of 100-200 sensors, which are distributed on a 2D plane of $100m \times 100m$, in which the BS is located at the center of the plane. Each sensor is powered by an alkaline rechargeable battery with the capacity $b = 1.5V \times 2A \times 3,600sec = 10.8KJ$ [11]. Before the simulation starts, the sensor residual energy re is randomly set between $0.1b$ and $1b$. Moreover, the energy consumption rate ec of each sensor randomly ranges between 0.05*J/s* and 0.5*J/s*. When the $ec = 0.5$*J/s* (*i.e.,* the maximal value), the residual lifetime of a sensor with full battery can reach 6 hours, thus we set the lifetime threshold $\theta_l = 6h$.

We assume that the battery capacity B of MC is $2,000KJ$, and the moving speed and the moving cost of MC are 5*m/s* and 50*J/m*, respectively [11]. By fitting our experiment data and referring to the hardware parameters of the equipment, the parameters of the charging model in Eq. (11) are set as: $\mu = 0.31$, $\beta = 0.053$, $G_m = 8$, $\theta_m = \pi/3$, $G_b = 1.856$, and $\theta_b = 2\pi/3$. According to the field experiment we performed in Fig. 2, we set the farthest charging distance of the main and back lobes as $2.6m$ and $1.3m$, respectively. The energy transmission power of the MC is set to $3W$.

To evaluate the performance of our proposed BACK algorithm, we compare it with the following charging algorithms.

Main Lobe Charging (MLC) [19] algorithm is a directional charging algorithm that only utilizes the main lobe. MLC considers the anisotropy of the received energy, and its objective is to jointly optimize the number of dead sensors and *EUE*.

Lifetime Maximization Charing (LMC) algorithm is also an directional charging algorithm that only utilizes the main lobe. However, the objective of LMC is to minimize the number of dead sensors. Therefore, LMC does not include the optimization algorithm based on the idea of exchanging sojourn locations.

Nearest-Job-Next with Preemption (NJNP) [16] is an on-demand charging algorithm for the single-sensor charging model. To save time and energy spent traveling, NJNP always serves the nearest sensor with a charging request.

B. Performance Comparisons

In this section, we evaluate the performance of our proposed scheme by comparing it with the three comparison algorithms under different number of sensors N and the beamwidth of the back lobe θ_b.

1) Impact of the number of sensors N: Fig. 9(a) shows the influence of the N on the number of dead sensors. As the number of sensors in the network increases, the N_{ds} yielded by all algorithms increases. However, we can see that BACK outperforms other algorithms by an average of 51.9%, and this advantage is even more evident when there is a greater number of sensors. This is because BACK is more likely to use the back lobe to charge more sensors simultaneously.

Fig. 9(b) compares another performance metric, *EUE*. BACK achieves 10.2% higher *EUE* than other algorithms on average. The rationale behind this is two-fold: (*i*) BACK makes full use of the energy radiated from the back lobe to charge more sensors simultaneously by adjusting the MC's orientation; (*ii*) the charging order exchanging-based *EUE* optimization algorithm can further shorten the traveling distance and reduce energy loss. Moreover, by comparing MLC and LMC, we find that although none of them take into account the energy radiated by the back lobe, LMC has a lower *EUE* due to the absence of *EUE* optimization.

Then, we measure the total traveling distance. From Fig. 9(c), we can see that NJNP has the best performance. The reason is that NJNP causes much larger N_{ds} than other algorithms do, the total traveling distance generated by NJNP is the shortest. Fig. 9(c) also shows that BACK has a shorter traveling distance than MLC and LMC. This is because full use of the back lobe can reduce the number of sojourn locations visited, thus effectively shortening the traveling distance.

2) Impact of the beamwidth of the back lobe θ_b: We fix the number of sensors at 150 and further investigate the impact of θ_b. Fig. 10(a) shows the comparison of N_{ds}. On average, BACK outperforms other algorithms by 47%. It also can be seen that with the increase of θ_b, the N_{ds} generated by all algorithms increases. This is because, with the increase of θ_b, the back lobe energy gradually disperses, making the energy intensity received by the sensors covered by the back lobe also decrease. Therefore, it is difficult for these sensors to obtain sufficient energy to guarantee their survival.

Fig. 10 compares the other two metrics, *EUE* and traveling distance. In Fig. 10(b), the *EUE* yielded by all algorithms decreases slightly as θ_b increases. The reason is that the more dispersed the back lobe energy is, the smaller the ratio of the energy received by sensors to the total energy radiated by the back lobe is, resulting in more energy loss in the charging process. Fig. 10(c) shows that the change of θ_b does not significantly influence the traveling distance of all algorithms.

Combining the results of Fig. 10, we can observe that the smaller the beamwidth of the back lobe, the more energy the sensor located in the back lobe region can receive from the more concentrated energy beam. Therefore, chargers equipped with antennas with larger back lobe gain can provide better charging service.

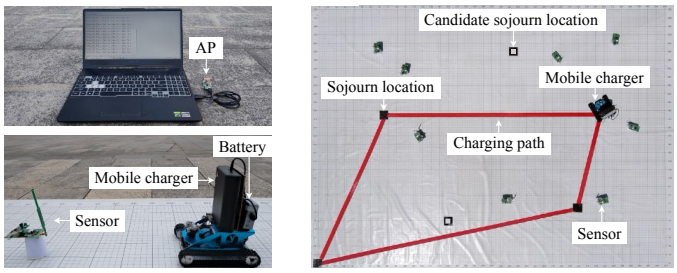

Fig. 11. Testbed.

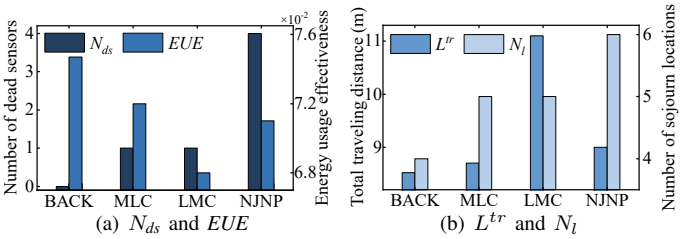

(a) N_{ds} and EUE (b) L^{tr} and N_l

Fig. 12. Performance comparisons.

VI. Field Experiments

In this section, we conduct field experiments to evaluate the performance of our algorithm. As shown in Fig. 11, our testbed consists of a robot car equipped with a TX91501 Powercast wireless charger, eight rechargeable sensors equipped with omnidirectional antennas, and an AP connecting to a laptop to report the collected data from the sensors. The robot car moves at a speed of $0.3m/s$ and consumes energy at a rate of $5.59J/m$ [17]. Sensors are deployed in a $400cm \times 300cm$ area, and their coordinates are $(70, 250)$, $(100, 225)$, $(115, 150)$, $(240, 75)$, $(275, 240)$, $(325, 75)$, $(340, 260)$, $(360, 160)$. Fig.11 also shows the actual charging path constructed by BACK.

Fig. 12 compares the four metrics, N_{ds}, EUE, L^{tr}, and N_l, where N_l is the number of sojourn locations in the charging path. Consistent with the simulation results, BACK outperforms the other three algorithms. The reason can be explained by Fig. 13, which depicts the charging paths constructed by the four algorithms. By making full use of the main and back lobes, we can observe that BACK covers more sensors at each sojourn location, which greatly reduces the number of sojourn locations visited, thus shortening the traveling distances and ensuring the survival of all sensors.

VII. Related Work

There are many studies on scheduling mobile chargers for WRSNs service, which can be divided into two categories based on the type of antenna the charger is equipped with: omnidirectional charging scheduling [5], [11], [12] and directional charging scheduling [19]–[21].

Omnidirectional charging scheduling: Most previous studies employ mobile chargers equipped with omnidirectional antennas to charge sensors. To achieve energy provisioning under complex weather conditions, Zhou et al. [5] proposed a self-sustained WSN by integrating multi-source energy harvesting with mobile charging. In [11], Liu et al. designed a partial charging mechanism to jointly optimize the number of dead sensors and the energy usage effectiveness. Xu et al. [12] studied the effective scheduling of multiple mobile chargers to charge sensors so that the maximum charging delay can be minimized. Nevertheless, omnidirectional antennas broadcast energy in all directions, resulting in low energy intensity within the charging range.

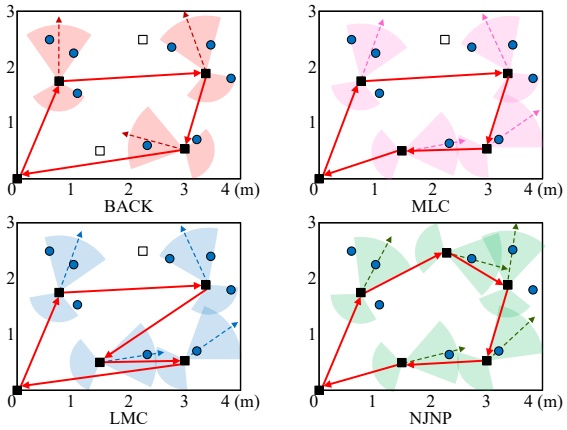

Fig. 13. Charging paths constructed by four algorithms.

Directional charging scheduling: There exist some studies employing chargers equipped with directional antennas. In [19], Lin et al. considered how to minimize charging delay by utilizing the anisotropic energy receiving property of sensors in directional charging. Sun et al. [20] concentrated on utilizing hybrid chargers and using freeloading directional chargers to recycle the wasted energy, so as to improve the energy efficiency of the whole network. Dai et al. [21] studied how to schedule a directional charger to recharge sensors in an arbitrary simple polygon with the charger only allowed to move along the polygon boundaries. However, they overlooked that the back lobe has significant energy, which is wasted.

VIII. Conclusion

The key novelty of this paper is to propose the first charging scheduling scheme which considers the back lobe in directional charging. The main contribution of this paper is to establish the directional charging model with the main and back lobes and verify the model by conducting experiments. Based on this model, we concentrate on jointly optimizing the number of dead sensors and energy usage effectiveness. To this end, we propose a scheme consisting of four sub-algorithms. Theoretical analysis shows that our scheme can approximate the minimum number of dead sensors and the maximum energy efficiency with a close ratio. Moreover, our simulation and field experimental results show that our proposed scheme significantly outperforms the existing algorithms.

Acknowledgment

This work is partially supported by the National Natural Science Foundation of China (62072320, 62002250, 62272328), the Natural Science Foundation of Sichuan Province (2022NSFSC0569), the Key R&D Program of Sichuan Province (22ZDZX0021). The authors would like to thank Dr. Baijun Wu for his useful feed-back and constructive comments, which helped us improve the quality and presentation of the paper.

REFERENCES

[1] A. Cohen, X. Shen, J. Torrellas, J. Tuck, and Y. Zhou, "Inter-disciplinary research challenges in computer systems for the 2020s," *National Science Foundation, USA, Tech. Rep*, 2018.

[2] Y. Hu, F. Qian, Z. Yin, Z. Li, Z. Ji, Y. Han, Q. Xu, and W. Jiang, "Experience: Practical indoor localization for malls," in *2022 28th Annual International Conference on Mobile Computing and Networking (MOBICOM)*, 2022, pp. 82–93.

[3] A. Kurs, A. Karalis, R. Moffatt, J. D. Joannopoulos, P. Fisher, and M. Soljačić, "Wireless power transfer via strongly coupled magnetic resonances," *science*, vol. 317, no. 5834, pp. 83–86, 2007.

[4] Y. Yang and C. Wang, *Wireless rechargeable sensor networks*. Springer, 2015.

[5] P. Zhou, C. Wang, and Y. Yang, "Design of self-sustainable wireless sensor networks with energy harvesting and wireless charging," *ACM Transactions on Sensor Networks*, vol. 17, no. 4, pp. 1–38, 2021.

[6] S. Wu, H. Dai, L. Xu, L. Liu, F. Xiao, and J. Xu, "Comprehensive cost optimization for charger deployment in multi-hop wireless charging," *IEEE Transactions on Mobile Computing*, 2022, early access.

[7] M. Zhao, J. Li, and Y. Yang, "A framework of joint mobile energy replenishment and data gathering in wireless rechargeable sensor networks," *IEEE Transactions on Mobile Computing*, vol. 13, no. 12, pp. 2689–2705, 2014.

[8] X. Fan, L. Shangguan, R. Howard, Y. Zhang, Y. Peng, J. Xiong, Y. Ma, and X. Li, "Towards flexible wireless charging for medical implants using distributed antenna system," in *2020 26th Annual International Conference on Mobile Computing and Networking (MOBICOM)*, 2020, pp. 1–15.

[9] L. M. Borges, F. J. Velez, and A. S. Lebres, "Survey on the characterization and classification of wireless sensor network applications," *IEEE Communications Surveys & Tutorials*, vol. 16, no. 4, pp. 1860–1890, 2014.

[10] S. He, J. Chen, F. Jiang, D. K. Yau, G. Xing, and Y. Sun, "Energy provisioning in wireless rechargeable sensor networks," *IEEE Transactions on Mobile Computing*, vol. 12, no. 10, pp. 1931–1942, 2013.

[11] T. Liu, B. Wu, S. Zhang, J. Peng, and W. Xu, "An effective multi-node charging scheme for wireless rechargeable sensor networks," in *2020 39th IEEE International Conference on Computer Communications (INFOCOM)*. IEEE, 2020, pp. 2026–2035.

[12] W. Xu, W. Liang, X. Jia, H. Kan, Y. Xu, and X. Zhang, "Minimizing the maximum charging delay of multiple mobile chargers under the multi-node energy charging scheme," *IEEE Transactions on Mobile Computing*, vol. 20, no. 5, pp. 1846–1861, 2021.

[13] T. Liu, B. Wu, W. Xu, X. Cao, J. Peng, and H. Wu, "Rlc: a reinforcement learning-based charging algorithm for mobile devices," *ACM Transactions on Sensor Networks*, vol. 17, no. 4, pp. 1–23, 2021.

[14] Y. Sun, C. Lin, H. Dai, P. Wang, L. Wang, G. Wu, and Q. Zhang, "Trading off charging and sensing for stochastic events monitoring in wrsns," *IEEE/ACM Transactions on Networking*, vol. 30, no. 2, pp. 557–571, 2022.

[15] R. Jia, J. Wu, J. Lu, M. Li, F. Lin, and Z. Zheng, "Energy saving in heterogeneous wireless rechargeable sensor networks," in *2022 41th IEEE International Conference on Computer Communications (INFOCOM)*. IEEE, 2022, pp. 1838–1847.

[16] L. He, L. Kong, Y. Gu, J. Pan, and T. Zhu, "Evaluating the on-demand mobile charging in wireless sensor networks," *IEEE Transactions on Mobile Computing*, vol. 14, no. 9, pp. 1861–1875, 2015.

[17] C. Wang, J. Li, F. Ye, and Y. Yang, "Recharging schedules for wireless sensor networks with vehicle movement costs and capacity constraints," in *2014 11th Annual IEEE International Conference on Sensing, Communication, and Networking (SECON)*. IEEE, 2014, pp. 468–476.

[18] Z. Wang, L. Duan, and R. Zhang, "Adaptively directional wireless power transfer for large-scale sensor networks," *IEEE Journal on Selected Areas in Communications*, vol. 34, no. 5, pp. 1785–1800, 2016.

[19] C. Lin, Z. Yang, H. Dai, L. Cui, L. Wang, and G. Wu, "Minimizing charging delay for directional charging," *IEEE/ACM Transactions on Networking*, vol. 29, no. 6, pp. 2478–2493, 2021.

[20] Y. Sun, C. Lin, H. Dai, P. Wang, J. Ren, L. Wang, and G. Wu, "Recycling wasted energy for mobile charging," in *2021 29th International Conference on Network Protocols (ICNP)*. IEEE, 2021, pp. 1–11.

[21] H. Dai, X. Wang, L. Xu, C. Dong, Q. Liu, L. Meng, and G. Chen, "Area charging for wireless rechargeable sensors," in *2020 29th International Conference on Computer Communications and Networks (ICCCN)*. IEEE, 2020, pp. 1–9.

[22] H. Dai, K. Sun, A. X. Liu, L. Zhang, J. Zheng, and G. Chen, "Charging task scheduling for directional wireless charger networks," *IEEE Transactions on Mobile Computing*, pp. 3163 – 3180, 2021.

[23] H. Dai, X. Wang, A. X. Liu, H. Ma, G. Chen, and W. Dou, "Wireless charger placement for directional charging," *IEEE/ACM Transactions on Networking*, vol. 26, no. 4, pp. 1865–1878, 2018.

[24] X. Wang, H. Dai, W. Wang, J. Zheng, N. Yu, G. Chen, W. Dou, and X. Wu, "Practical heterogeneous wireless charger placement with obstacles," *IEEE Transactions on Mobile Computing*, vol. 19, no. 8, pp. 1910–1927, 2020.

[25] H. Dai, X. Wang, X. Lin, R. Gu, S. Shi, Y. Liu, W. Dou, and G. Chen, "Placing wireless chargers with limited mobility," *IEEE Transactions on Mobile Computing*, 2021, early access.

[26] N. Yu, H. Dai, G. Chen, A. X. Liu, B. Tian, and T. He, "Connectivity-constrained placement of wireless chargers," *IEEE Transactions on Mobile Computing*, vol. 20, no. 3, pp. 909–927, 2021.

[27] C. A. Balanis, *Antenna theory: analysis and design*. John wiley & sons, 2015.

[28] Powercast, "Online," http://www.powercastco.com.

[29] Alien Technology, "Online," http://www.alientechnology.com.

[30] Taoglas, "Online," http://taoglas.com.

[31] N. Javanbakht, R. E. Amaya, J. Shaker, and B. Syrett, "Side-lobe level reduction of half-mode substrate integrated waveguide leaky-wave antenna," *IEEE Transactions on Antennas and Propagation*, vol. 69, no. 6, pp. 3572–3577, 2021.

[32] N. Javanbakht, M. S. Majedi, and A. R. Attari, "Thinned array inspired quasi-uniform leaky-wave antenna with low side-lobe level," *IEEE Antennas and Wireless Propagation Letters*, vol. 16, pp. 2992–2995, 2017.

[33] F. Chen, H. Hu, R. Li, Q. Chu, and M. J. Lancaster, "Design of filtering microstrip antenna array with reduced sidelobe level," *IEEE Transactions on Antennas and Propagation*, vol. 65, no. 2, pp. 903–908, 2017.

[34] M. Z. Hasan and H. Al-Rizzo, "Beamforming optimization in internet of things applications using robust swarm algorithm in conjunction with connectable and collaborative sensors," *Sensors*, vol. 20, no. 7, p. 2048, 2020.

[35] T. Bai and R. W. Heath, "Coverage and rate analysis for millimeter-wave cellular networks," *IEEE Transactions on Wireless Communications*, vol. 14, no. 2, pp. 1100–1114, 2015.

[36] A. Thornburg, T. Bai, and R. W. Heath, "Performance analysis of outdoor mmwave ad hoc networks," *IEEE Transactions on Signal Processing*, vol. 64, no. 15, pp. 4065–4079, 2016.

[37] E. Aarts and J. Lenstra, "The traveling salesman problem: A case study," in *Local Search in Combinatorial Optimization*. Wiley, 1997, pp. 215–310.

[38] C. Engels and B. Manthey, "Average-case approximation ratio of the 2-opt algorithm for the tsp," *Operations Research Letters*, vol. 37, no. 2, pp. 83–84, 2009.